CONSERVATION of APOLIPOPROTEIN A-I's CENTRAL DOMAIN STRUCTURAL ELEMENTS UPON LIPID ASSOCIATION ON DIFFERENT HDL SUBCLASSES

Michael N. Oda[§], **Madhu S. Budamagunta**[‡], **Ethan G. Geier**[§], **Sajiv H. Chandradas**[§], **Baohai Shao**[#], **Jay W. Heinecke**[#], **John C. Voss**[‡], and **Giorgio Cavigiolio**[§,*]
[§]Children's Hospital Oakland Research Institute, Oakland, California 94609, USA

[‡]Department of Biochemistry and Molecular Medicine, University of California, Davis, CA 95616

[#]Department of Medicine, University of Washington, Seattle, Washington 98195

Abstract

The antiatherogenic properties of apolipoprotein A–I (apoA-I) are derived, in part, from lipidation state dependent structural elements that manifest at different stages of apoA-I's progression from lipid-free protein to spherical high density lipoprotein (HDL). Previously, we reported the structure of apoA-I's N-terminus on reconstituted HDL (rHDL) of different sizes. We have now investigated at the single residue level the conformational adaptations of three regions in the central domain of apoA-I (119–124, 139–144, and 164–170) upon apoA-I lipid binding and HDL formation. An important function associated with these residues of apoA-I is the activation of lecithin:cholesterol acyltransferase (LCAT), the enzyme responsible for catalyzing HDL maturation. Structural examination was performed by site-directed tryptophan fluorescence and spin-label electron paramagnetic resonance spectroscopies for both the lipid-free protein and rHDL particles of 7.8, 8.4, and 9.6 nm diameter. The two methods provide complementary information on residue side chain mobility and molecular accessibility, as well as polarity of the local environment at the targeted positions. The modulation of these biophysical parameters yielded new insight into the importance of structural elements in the central domain of apoA-I. In particular, we determined that the loosely-lipid-associated structure of residues 134–145 is conserved in all rHDL particles. Truncation of this region completely abolished LCAT activation but did not significantly affect rHDL size, reaffirming the important role of this structural element in HDL function.

Human high density lipoprotein (HDL) is a lipid-protein complex composed of approximately fifty proteins and a heterogeneous neutral lipid core (1, 2). Multiple functions such as cellular cholesterol homeostasis, plasma cholesterol transport, and anti-inflammatory, anti-oxidant, and anti-thrombotic activities contribute to HDL's antiatherogenic effect (3–8). Although these activities may be catalyzed by an array of HDL resident proteins, HDL's function is influenced by the structure of the main protein scaffold, primarily composed of apolipoprotein A–I (apoA-I) (9).

[*]To whom correspondence should be addressed: Giorgio Cavigiolio, Children's Hospital Oakland Research Institute, 5700 Martin Luther King Jr. Way, Oakland, CA 94609, Tel.: +1 (510) 450-7630, Fax.: +1 (510) 450-7910, gcavigiolio@chori.org.

According to the double belt model for nascent HDL, the initial state of HDL during biogenesis, apoA-I assumes a curved amphipathic -helical ring structure where two apoA-I molecules are associated in an antiparallel fashion on the perimeter of a phospholipid bilayer. The model was originally derived from the crystal structure of an N-terminally truncated lipid-free apoA-I (10) and has been confirmed by several laboratories using *a priori* modeling (11) and an array of biophysical methods (12–27). Wu et al. proposed an alternative model for nascent 9.6 nm diameter HDL, termed the double super helix model, wherein apoA-I assumes an asymmetrical helical shape that wraps around a central micellar lipid phase (28). However, the double super helix model has been the subject of considerable debate (29, 30). Recently, Jones, et al. (30) used molecular dynamics, fluorescence spectroscopy, and electron microscopy to test this model. The preponderance of evidence refuted the double super helix model and further substantiated the double belt model.

Within the various models based on the double belt scaffold, specific structural details have also been the object of scrutiny and debate. Several computational and experimental studies detected discontinuities in the -helical secondary structure of apoA-I on nascent HDL; however, there is little agreement on the position, size, and structure of these regions (19, 22, 24, 31–34). The loose lipid association of these non-helical segments in the central domain are postulated to serve a functional role relevant to lecithin:cholesterol acyltransferase (LCAT) activation (22, 24, 33). In 2006 we identified a non- -helical region (134–145) in the central domain of apoA-I in 9.6 nm diameter HDL by site directed spin label electron paramagnetic resonance (SDSL-EPR) and fluorescence analysis, and proposed the 'looped-belt' model (22). We speculated that this structural element is a 'portal' facilitating LCAT access to acyl chain substrate during the cholesterol-acyl transfer reaction. This hypothesis has been corroborated recently by molecular dynamic experiments (33). In contrast, Wu et al., (24) proposed the 'solar-flares' model, wherein a non-lipid-associated loop region spans residues 159 and 180 and no -helical discontinuity was observed for region 134–145. The veracity of the 'solar-flares' model was evaluated by molecular dynamics experimentation (35) and the loop conformation of residues 159–180 was found to be unstable. The recent hydrogen-deuterium exchange mass-spectrometry study by Chetty et al. also provides evidence that residues 158–180 on 9.6 nm rHDL are -helical and do not adopt a loop conformation (34).

While the first conformational analysis of plasma isolated HDL subclasses was recently published (9), a majority of HDL structural information is based on studies of reconstituted HDL (rHDL), which have largely been focused on 9.6 nm diameter discoidal particles. However, plasma nascent HDL is a heterogeneous population of particles of 7.5 to 17.0 nm diameter (2, 27, 36, 37). To gain a more functional understanding of the role of specific apoA-I structural features in the biogenesis and metabolism of HDL, knowledge of their representation on different sized rHDL is essential. Recently, Chetty et al. investigated the secondary structure of apoA-I on rHDL and identified the position of -helical regions within apoA-I on 9.6 and 7.8 nm rHDL particles (34). Although exhaustive, these results are derived from the overall thermodynamic stability of peptide segments, and do not define the structure of apoA-I at the single-residue level. Examination of specific structural elements at the single-residue level is needed to understand the structure-function relationship of apoA-I on different HDL subclasses. Such knowledge would provide insight into the functional consequences of specific molecular modifications of apoA-I and their contribution to HDL dysfunction-associated pathologies like cardiovascular disease.

We recently investigated the conformation of apoA-I's N-terminus on different sized rHDL by SDSL-EPR analysis at the single-residue level and found that specific structural elements are present in a particle size-dependent fashion. Here, we extended our analysis to three

regions of apoA-I's central domain through a combination of SDSL-EPR and fluorescence spectroscopies. Residues 139–144 (loop segment in the 'looped-belt' model), 164–170 (loop segment in the 'solar-flares' model), and 119–124 (amphipathic -helical lipid-associated residues in both models) were analyzed by tryptophan and spin-label scanning in the lipid-free protein and HDL subclasses of 7.8, 8.4 and 9.6 nm diameter. This array of structural approaches allowed us to differentiate between structural features of apoA-I versus chemical features of the protein. Because the 'solar flares' model was proposed on the basis of hydrogen-deuterium exchange analysis, we hypothesize that this data more likely represented the local chemistry/pK$_a$ of the protein rather than a direct structural aspect of apoA-I. Our structural analysis, in combination with the functional characterization of truncated apoA-I variants provides new insight into the role of specific central domain structural elements in nascent HDL particles biogenesis.

EXPERIMENTAL PROCEDURES

Materials

Thio-specific nitroxide spin-label (MTS; (1-Oxyl-2,2,5,5-tetramethylpyrroline-3-methyl) methanethiosulfonate) was a generous donation from Dr. K. Hideg (University of Pecs, Hungary). 1-palmitoyl-2-oleoyl-sn-glycero-phosphocholine (POPC) was from Avanti Polar Lipids, Inc. (Alabaster, AL).

Production of Recombinant Protein and Spin-labeling

Twenty-one single Cys, nineteen single Trp, and two central region truncation apoA-I cDNA variants were produced using either primer-directed PCR mutagenesis or the megaprimer PCR method (38). In the single Trp-variants, endogenous Trp fluorescence was eliminated by substituting the four native Trp residues (8, 50, 72, and 108) with Phe as described (22, 39). The mutations were verified by dideoxy automated fluorescent sequencing. The proteins were expressed in BL21 *E. coli* (InVitrogen) and purified as previously reported (40). MTS spin-labeling of cysteines was performed as described (41, 42). Protein samples were stored in Tris buffered saline (TBS; 8.2 mM Tris, 150 mM NaCl, 1 mM EDTA, pH 7.4). Protein purity (>95%) was confirmed by SDS-PAGE analysis (Fig. 1A).

Preparation of apoA-I-POPC Complexes

Spin-labeled apoA-I, single-Trp apoA-I, and truncated apoA-I-containing rHDLs were prepared by the deoxycholate method (43–45). Different rHDL subclasses of 7.8, 8.4, 9.6, 12.2, and 17.0 nm diameter were isolated as described (45). Briefly, POPC, unesterified cholesterol, and proteins were combined in molar ratios of 160:8:1 to generate 17.0 and 12.2 nm rHDL, 80:4:1 to yield preferentially 9.6 nm rHDL, and 30:2:1 to produce 8.4 and 7.8 nm rHDL. Final rHDL protein-lipid composition was as described (45). The rHDL subclasses were isolated by size exclusion chromatography on a Superdex 200 prep grade XK 16/100 column (GE Biosciences Inc.). The size and purity of the rHDL subclasses were confirmed by non-denaturing gradient gel electrophoresis (NDGGE) (Fig. 1B). rHDL samples were stored at 4 °C in TBS (pH 8.0) and used for spectroscopic analysis within one week from preparation. For apoA-I: 124–155, the lipidation yields were low and the product mixtures very heterogeneous at lipidation molar ratios of 30:1 and 80:1.

Fluorescence Spectroscopy

To investigate the local environment of residues in the central domain of apoA-I we produced apoA-I variants in which all four native Trp residues were substituted with Phe and a single-Trp was introduced at strategic positions (Supplemental Fig. S1). Steady-state

fluorescence spectra of lipid-free proteins and corresponding rHDL particles were recorded at 20 °C on a Horiba Jobin-Yvon Fluoromax-4 spectrofluorometer, using a 1.5-nm slit width for both the excitation and emission monochronomators. Samples in TBS were normalized at 0.5 mg/mL protein concentration and excited at 295 nm. Fluorescence spectra were recorded over the 300–420 nm range. The emission $_{max}$ of Trp reports on the polarity of the local environment. According to Burstein et al., Trp residues can be classified as: class I (330–332 nm), in apolar protein regions; class II (340–342 nm), on protein surface but with limited solvent exposure; class III (350–352 nm), solvent exposed (46). Furthermore, $_{max}$ has been largely employed as a means of determining Trp 'lipid-exposure' in lipoproteins (47, 48). It has been empirically established that $_{max}$ in the 324–335 nm range indicate residues in contact with lipids or buried in hydrophobic protein pockets, whereas $_{max}$ larger than 345 nm is suggestive of Trp facing the solvent exposed side of amphipathic -helices (19, 49). See Supplemental Fig. S2 for a representative example of fluorescence emission spectra of a single-Trp protein variant (L144W) in the lipid-free state and on rHDL.

Fluorescence Quenching Analysis

Potassium iodide quenching was employed as a means of establishing positional solvent accessibility, as described (49, 50). Sodium thiosulfate (1 mM) was added to a freshly prepared stock solution of KI (4 M) as an antioxidant to prevent formation of triiodide ion (I_3^-) (51). To lipid-free protein or rHDL samples (0.5 mg/ml in apoA-I) the KI stock solution was added in small increments to final KI concentrations from 0 to 1.75 mM. An emission fluorescence spectrum was collected after each increase in KI concentration and the emission intensity was corrected for the dilution due to the corresponding volume increase. The Trp fluorescence collisional quenching by KI was analyzed by Stern-Volmer regression, $F_0/F = 1 + K_{sv}[Q]$, where F_0 and F are the maximum emission intensities at an appropriate emission wavelength (in our case $_{max}$) in the absence and presence of KI, respectively. [Q] is the molar concentration of the quencher (52). The Stern-Volmer quenching constant K_{sv} is derived as slope of the F_0/F versus [Q] plot. K_{sv} is proportional to the solvent accessibility of the Trp residue. For totally exposed Trp residues, in the absence of electrostatic or viscosity effects, $K_{sv}=12 M^{-1}$; on the other hand, for totally protected Trp residues $K_{sv}=0 M^{-1}$ (53). For apolipoproteins, K_{sv} values <2.5 have been empirically assigned to Trp residues in nonpolar environment and K_{sv} values >3.5 M^{-1} to solvent exposed Trp residues (49).

Electron Paramagnetic Resonance (EPR) Spectroscopy

100 G width EPR spectra were collected on a JEOL X-band EPR spectrometer fitted with a loop-gap resonator (54, 55). Aliquots (5–6 μl) of protein or lipoprotein samples (60 μM spin-labeled protein) were loaded into quartz microcapillaries sealed at one end and placed in the resonator for EPR measurements. Spectra were acquired at room temperature (20–22 °C) from a single 2-min scan over a field of 100 G at a microwave power of 4 mW with a modulation amplitude optimized to the natural line width of the individual spectrum (1.0 – 1.6 G). Normalization was calculated from the sample alleviated from broadening by integrating the spectrum obtained in the presence of sodium-dodecyl sulfate (SDS; 2 % (w/v)).

The motional freedom of the spin-label determines the spectral features of the X-band EPR spectrum, thus analysis of the spectra of a series of consecutive spin-labeled side chains provides information on the level of local structural order. We measured the mobility parameter, $^{-1}$, of single spin-labeled apoA-I variants as the inverse of the central line width of the EPR spectra and analyzed the results in the context of an amphipathic -helix model. Restriction in mobility may arise from intra- or intermolecular protein-protein contacts and, in lipoproteins, by protein-lipid contacts.

Molecular accessibility to the spin-label was probed by measuring the EPR signal quenching by two diffusible relaxation agents, the polar chromium oxalate (CrOx) and the non-polar oxygen (O_2). The accessibility parameter ($\Pi_{1/2}$) of the two quenchers were calculated using software provided by C. Altenbach as described (41, 42, 56). The polarity index (or contrast function, Φ) was calculated as the logarithmic ratio of the $\Pi_{1/2}$ values of the polar and non-polar quenchers. For lipid-associated proteins the polarity index provides a measure of the membrane penetration depth of the spin-label (57, 58). Residues with $\Phi > -0.5$ were scored as lipid buried, whereas residues with $\Phi < -1.5$ where considered largely solvent exposed. Intermediate Φ values were assigned to residues in the water-lipid interface (59, 60).

LCAT Activation Assay

LCAT activation by rHDL was monitored by following the conversion of cholesterol to cholesteryl ester as previously reported (45, 61). Briefly, five rHDL subclasses were generated as described above but in the absence of unesterified cholesterol, and were characterized by NDGGE and chemical composition (POPC:apoA-I ratio). [1,2-^{3}H]-cholesterol was introduced exogenously into the rHDL complexes. rHDL samples (2 μg in apoA-I) were diluted in TBS and equilibrated with radiolabeled cholesterol by incubation at 37 °C for 30 min with 1.39 pmol of [1,2-^{3}H]-cholesterol (57.6 Ci/mmol, PerkinElmer Life and Analytical Sciences Inc., Boston, MA). The mixtures were incubated at 37 °C for 1 h in presence of 5 mg/ml (final) BSA and 4 mM (final) β-mercaptoethanol. LCAT (50 ng) was added and the reaction was incubated for 1 h at 37 °C; the reactions were terminated by the addition of 1 ml absolute ethanol. Lipids were extracted with hexane and the cholesterol and cholesteryl ester were separated by thin layer chromatography using hexane:ethyl ether:acetic acid (108:30:1.2, v:v:v) as the solvent phase. The lipid spots were visualized under iodine vapor and recovered for scintillation analysis (Beckman Coulter LS 6500 multi-purpose scintillation counter, Fullerton, CA). The LCAT reaction conditions were chosen on the basis of the linear response range of LCAT.

Statistical Analysis

Results are the average of at least three independent experiments, in which the process of protein expression, labeling, HDL reconstitution, rHDL purification, and spectroscopic acquisition was repeated. Because there was a small and consistent ($\leq 10\%$) Standard Deviation for a majority of the data, error bars are not reported in Fig. 2–5 for the sake of ease of readability. Student's two-tailed, unpaired *t*-test was used for statistical analyses and $P < 0.05$ was considered significant.

Assessment of ApoA-I Conformation

To survey the structural adaptation of apoA-I from lipid-free to rHDL particles of different size, 19 residues in three regions of the central domain of apoA-I were mutated to single Trp (residues 119–124, 139–144, and 164–170), and 21 residues were mutated to single Cys (residues 119–124, 133, 139–144, and 146). Single cysteine bearing apoA-Is were spin-labeled with a nitroxide spin-label for EPR analysis. Single-Trp or single spin-label containing protein variants were reconstituted into HDL particles of 7.8, 8.4 (for positions 139–143 and 164–170), and 9.6 nm diameter. Lipid-free and rHDL samples were analyzed using two physical methods, fluorescence spectroscopy and EPR. Each apoA-I residue examined was evaluated on four metrics of protein conformation: 1) **local polarity** was assessed from the maximum fluorescence emission wavelength (λ_{max}) of single Trp bearing apoA-I mutants; 2) **solvent accessibility** was measured by the susceptibility of single Trp bearing apoA-Is to fluorescence quenching by potassium iodide; 3) **residue polarity** was evaluated by measuring the molecular accessibility ($\Pi_{1/2}$) of two diffusible relaxation agents by EPR, and the derived polarity index (Φ). For lipoproteins, Φ is dependent upon the

penetration depth of the spin-label into the phospholipid bilayer; and 4) **residue mobility** was determined from the line-width ($^{-1}$) of the EPR spectrum. These data were then modeled in the context of an ideal amphipathic -helix of 11/3 (11 residues) or 18/5 (18 residues) pitch (Supplemental Fig. S3). The identification of solvent-exposed surface and the periodicity of the backbone structure were determined from the modulation of these parameters as a function of sequence position.

RESULTS

Selection of scanned positions within apoA-I

The residues selected for analysis represent three unique portions of apoA-I on HDL. Amino acids 139–144 are within a loop region in the 'looped-belt' model (residues 134–145) (22). Residues 164–170 are in the center of a loop region in the 'solar-flares' model (residues 159–180) (24). In contrast, residues 119–124 have been reported to form a lipid-associated amphipathic -helical structure on 2-apoA-I-containing rHDL (20–25, 34) and were evaluated as a "control" set of residues. All three regions contain a single Pro and span an amphipathic -helical junction, traditionally referred as H4–H5, H5–H6 and H6–H7 for residues 119–124, 139–144, and 164–170, respectively (Supplemental Fig. S1) (62, 63).

Trp fluorescence scanning

To assess the secondary structure of residues 119–124, 139–143, and 164–170 of apoA-I, we determined the polarity of the local environment surrounding these residues by Trp scanning fluorescence analysis. To enable this survey, we substituted all four Trp residues of wild-type apoA-I with Phe and produced nineteen single-Trp variants. The protein variants were used to reconstitute 7.8 and 9.6 nm rHDL. For residues 139–144 and 164–170, 8.4 nm rHDL particles were also generated. The emission $_{max}$ of lipid-free and rHDL-associated proteins were evaluated. Upon lipid binding, the $_{max}$ for the resident Trp was blue shifted up to 14 nm (Supplemental Fig. S2). This blue shift is the hallmark of changes in local polarity experienced by the tryptophan (52).

The $_{max}$ of the residues examined (Fig. 2) exhibit consistent periodic patterns, yielding three primary observations. First, for a majority of the nineteen residues, there were no significant differences in $_{max}$ between lipid-free and HDL-associated apoA-I. Thus the environments surrounding the examined residues have similar polarity regardless of whether protein-protein or protein-lipid interactions are predominant.

Second, local polarity was not significantly different among the three rHDL subclasses analyzed. Only residues 119, 142, 143, and 167 showed small differences among the various rHDL subclasses, which however did not affect the general score for the four residue environments (i.e. solvent exposed for residues 142 and 143; apolar for residues 119 and 167).

Third, the general pattern of $_{max}$ periodicity is consistent with a lipid-associated amphipathic -helical model for all three regions in the three rHDL subclasses analyzed (Fig. 2). Only the $_{max}$ of residue 170 is inconsistent with a residue within a lipid-associated amphipathic -helix, in which it would be deeply buried in the lipid bilayer. Although upon lipid binding the $_{max}$ of Trp 170 (336 and 337 nm for 7.8 and 9.6 nm rHDL, respectively) approaches the value empirically determined as indicative of a residue transitioning from polar to non-polar environments (335 nm), this blue-shift is too small to reclassify the residue as residing in a non-polar environment.

Solvent accessibility by Trp scanning fluorescence quenching

The relative solvent exposure of the central domain residues was measured by potassium iodide quenching of Trp fluorescence for the nineteen single-Trp apoA-I variants in the lipid-free and HDL-associated forms. Consistent with the local polarity results obtained by Trp $_{max}$ scanning, solvent accessibility was not significantly different between lipid-free and HDL-associated apoA-I. Thus the native folding of lipid-free apoA-I determines local polarity and solvent accessibility for the protein segments under analysis that are similar to the local environment occurring upon binding of the protein to the edge of a phospholipid bilayer. It is important to notice that protein-protein interactions in lipid-free apoA-I can be intra- or inter-molecular. In the current experimental conditions (~18 μM), lipid-free apoA-I is self-associated and inter-molecular contacts may contribute to the folding of the protein. This is particularly true for Trp to Phe apoA-I variants that exhibit higher levels of self-association compared to wild-type apoA-I (64) or the single Cys mutants used for EPR analysis.

In the rHDL particles analyzed, the periodicity of Stern-Volmer constants (K_{sv}) (Fig. 3) for residues 119–124 was compatible with the lipid-associated amphipathic -helical model and similar to the trend observed for Trp fluorescence $_{max}$ (Fig. 2). In contrast, K_{sv} for three (140, 142 and 143) of the six residues in region 139–144 were too low to correspond with an orientation towards a solvent exposed environment and inconsistent with a lipid-associated amphipathic -helical conformation. Thus the K_{sv} results do not support an ideal lipid-associated amphipathic -helical structure for residues 139–144. No significant differences in K_{sv} were observed for residues 119–124 and 139–143 for different rHDL subclasses, which is in agreement with the fluorescence $_{max}$ analysis results.

The K_{sv} results for residues 164–170 were unanticipated. First, the K_{sv} constants of residue 168 in the lipid-free protein and 9.6 nm rHDL (12.48 and 12.12 M^{-1}, respectively) were much higher than any other residues analyzed and similar to totally exposed Trp (53). Second, unique in the whole series, K_{sv} of five (164, 165, 166, 167, and 168) out of seven residues in region 164–170 were significantly different between 7.8 and 9.6 nm rHDL. Third, although K_{sv} of all residues in 7.8 nm rHDL were compatible with the lipid-associated amphipathic -helical model, K_{sv} of two residues (164, $K_{sv}=2.75$ M^{-1}, and 165, $K_{sv}=1.19$ M^{-1}) in 9.6 nm rHDL did not match the solvent accessible prediction of the model.

Combined, the fluorescence results ($_{max}$ and K_{sv}) indicate that residues 119–124 form a lipid-associated amphipathic -helix in all rHDL particles analyzed. In contrast, while fluorescence $_{max}$ results for residues 139–144 are compatible with an amphipathic -helical structure, K_{sv} analysis does not support the same conclusion. The fluorescence results for residues 164–170 are consistent with a lipid-associated amphipathic -helix in 7.8 nm rHDL, but some K_{sv} results are outliers both in absolute value (168) and in trend (164 and 165) for an amphipathic -helix structure in 9.6 nm rHDL. The apparently contradictory K_{sv} results for residues 164–170 may have been produced by the unique charge properties of this region.

Side chain polarity determined by EPR

The polarity of residue side chains labeled with a nitroxide spin label can be quantified from the relative collision frequency of the nitroxide with polar (CrOx) or non-polar (O_2) relaxation agents. The polarity index ( ) was calculated for all residues analyzed and used to generate regional topological maps of apoA-I (see Experimental Procedures). Specifically, the secondary structure was inferred from the periodicity of as a function of residue

number; amphipathic α-helical structures typically display a periodicity of 3.6, whereas β-strand structures exhibit an alternating periodicity.

Interestingly, all residues in regions 119–124 and 139–144 of the lipid-free protein exhibited a very negative (<–1.87) polarity index (very polar environment) (Fig. 4). In contrast, the range of polarity index for residues 164–170 was much higher (less polar) (Π, (–0.02)–(–2.86)) compared to residues 119–124 (Π, (–2.11)–(–3.34)) and 139–144 (Π, (–1.87)–(–2.64)). In particular, 167 was the only residue out of nineteen with polarity index >–0.5 (Π =–0.02).

Upon lipid binding, the polarity index of ten out of twelve residues in regions 119–124 and 139–144 increased. Only the polarity index of residues 139 and 143 did not change significantly (Fig. 4). In contrast, although the polarity index of five out of seven residues within region 164–170 (164, 166, 167, 169, and 170) increased, residues 165 and 168 (lipid-free Π, –1.69 and –2.69, respectively) significantly decreased in polarity index when the protein was HDL-associated (7.8 nm Π, –2.46 and –3.33, respectively; 9.6 nm Π, –2.12 and –3.29, respectively).

The polarity index pattern of the residues in region 119–124 and 164–170 is consistent with these residues assuming a lipid-associated amphipathic α-helical conformation on all rHDL sizes analyzed. In contrast, within region 139–144, two (residues 142 and 144) out of the six positions examined bore polarity values inconsistent with an interpretation indicating that these residues assume an amphipathic α-helical structure, as position 142 is too hydrophobic for an aqueous exposed residue and 144 is too hydrophilic for a lipid-embedded position. This is true for 7.8, 8.4, and 9.6 nm rHDL, with sites 142 and 144 having Π values of (–0.37, –0.48, –0.54) and (–1.84, –0.58, –0.58) for the three size rHDLs, respectively. In contrast the polarity indexes of analogous residues in region 119–124 (positions 119 and 124, Π = 0.74, 1.19 for 7.8 nm rHDL and Π = –2.62, –2.28 for 9.6 nm rHDL) are consistent with a lipid-associated amphipathic α-helix conformation.

Steric environment of residue side-chains

Local steric constraints imposed upon a spin-labeled side chain can be quantified from the inverse of the EPR spectra central peak-to-peak width, which defines the mobility parameter (ΔH^{-1}). The patterns of side chain mobility (ΔH^{-1}) (Fig. 5) and polarity index (Π) (Fig. 4) for all residues examined are strikingly similar. This observation is even more remarkable considering that the two datasets are based on different physical properties and derived from independent experiments.

In the absence of lipid, a majority of the nineteen residues examined were highly mobile (ΔH^{-1} ≥ 0.27). Although residues 119, 167, 169, and 170 were partially restricted in mobility, only ΔH^{-1} of residue 167 was below 0.25, the value empirically selected for marking the transition between mobile and immobilized residues (Fig. 5).

The conformational adaptation that occurs upon apoA-I lipid binding produced significant changes in residue mobility. With the exception of position 143, all residues in the 119–124 and 139–144 regions exhibited reduced side chains mobility on all rHDL particles analyzed (Fig. 5). Upon lipid binding, residues 121 and 124 retained a high level of mobility (ΔH^{-1} ≥ 0.36), as expected for residues that are solvent oriented within a lipid-associated amphipathic α-helical structure. In contrast, the mobility of residues 119 and 123 was very low on all rHDL particles (ΔH^{-1} ≤ 0.23), consistent with the orientation of these residues towards a lipid environment. Mobility of residues 120 and 122 was also significantly lower in all lipid-bound forms of the protein (ΔH^{-1} ≤ 0.30 and ΔH^{-1} ≤ 0.31, respectively). Whereas reduction in mobility of residue 122 can be accounted for by the proximity of this residue to

the water-lipid interface, the mobility of residue 120 in 9.6 nm rHDL ($^{-1}$=0.26) is unexpectedly low for a residue oriented towards solvent in an lipid-associated amphipathic -helix.

Notably, the side-chain mobility for residues 139–144 of lipid-free apoA-I was smaller ($^{-1}$ ranging between 0.31 and 0.39; average, 0.35) than for residues 119–124 ($^{-1}$ ranging between 0.26 and 0.47; average, 0.37). Although lipid binding produced a drastic reduction of side-chain mobility ($^{-1}$ ranging from −0.04 to −0.15), the interpretation of this change is not straightforward. On an amphipathic -helix, mobilities of residue 141 and 144 are anticipated to be the most affected by lipid-binding. Interestingly, reduction in mobility of reside 141 and 144 ($^{-1}$, −0.08 and −0.04, respectively) was not as large as for the analogous residues 122 and 123 ($^{-1}$, −0.09 and −0.11, respectively) in the 119–124 region. Furthermore, $^{-1}$ of residue 144 was significantly reduced on 9.6 nm rHDL ($^{-1}$, −0.04) but not on 7.8 nm ($^{-1}$, +0.01) and 8.4 nm ($^{-1}$, −0.01) rHDL, compared to the lipid-free protein. Residues 140 and 142, although predicted by the lipid-associated amphipathic -helical model to be marginally affected by lipid-interaction, experienced the largest mobility reduction of all residues examined ($^{-1}$, −0.15 and −0.13, respectively). Furthermore, the mobility of residue 143, predicted to reside on the apolar face of an amphipathic -helix, was unaffected by lipid binding; whereas the mobility of the highly unrestricted residue 139 was significantly reduced in all lipid-bound forms, which is inconsistent with the prediction of an amphipathic -helical model.

The overall side-chain mobility of residues 164–170 in the lipid-free protein was considerably lower compared to residues 119–124 and 139–144. Notably, the motion of residue 167 was highly restricted in the lipid-free state ($^{-}$=0.20), suggesting strong immobilization due to protein contacts of a buried site (65).

Due to the lower mobility of residues 164–170 in the lipid-free protein, compared to residues 119–124 or 139–144, lipid binding yielded an assortment of mobility changes, whereas for residues 119–124 and 139–144 lipid binding led to wholesale reductions in side chain mobility. Specifically, 3 out of 7 residues between positions 164 and 170 exhibited a significant increase in mobility (residues 165 and 168) or no changes at all (residue 169). Residue mobilities on rHDL particles of all sizes were consistent with a lipid-associated amphipathic -helical conformation for this region (164–170). Residues 166, 167, and 170, predicted to be in contact with lipids based on their positions within an amphipathic -helix, were indeed the least mobile ($^{-1}$ 0.26). Also consistent with an amphipathic -helical conformation, residues 165 and 168 were highly mobile ($^{-1}$ 0.34), indicating solvent exposure. Finally, residues 164 and 169 exhibited intermediate mobility values ($^{-1}$, 0.26 and 0.28, respectively), consistent with a position at the oil-water interface, as predicted by the amphipathic -helical model.

Combined, the EPR results (side-chain mobility and polarity index) support three primary conclusions. 1) In the lipid-free protein, residues in regions 119–124 and 139–144 are not restricted in motion or polar solvent accessibility; whereas two residues in region 164–170 exhibit restricted mobility and polar relaxation agent accessibility ($_{CrOx}$, 0.042 and 0.194 for residue 167 and 170, respectively). 2) In the lipid-bound states, regions 119–124 and 164–170 fit a lipid-associated amphipathic -helical model; whereas residues 139–144 do not exhibit an ideal amphipathic -helical pattern. 3) Notably, the side-chain mobility and polarity index of a majority of the nineteen residues analyzed do not significantly vary for different HDL subclasses. The spectra of spin-labels at the other two (133 and 146) of the three key positions identified by the 'looped-belt' model (residues 133, 139, and 146) were also virtually identical in 7.8 and 9.6 nm rHDL (Fig. 6).

rHDL particle formation and LCAT activation by central loop truncation variants

To test the hypothesis that residues 134–145 are essential for LCAT activation but contribute minimally to the overall structure of 2-apoA-I-containing rHDL particles (7.8, 8.4, 9.6 nm rHDL, (45)), we produced two apoA-I truncation variants (apoA-I: 134–145 and apoA-I: 124–155) in which 12 and 22 residues in the central domain were deleted. Removal of a non-lipid-associated portion of apoA-I would have a minimal effect on the size of the rHDL particles. In contrast, elimination of residues that form a portion of the 'belt' circumscribing the HDL particle perimeter would have a noticeable effect on the size of the reconstituted particles.

Wild-type apoA-I was combined in various ratios with POPC to reconstitute HDL particles of five sizes, 7.8, 8.4, 9.6, 12.2, and 17.0 nm (see Experimental Procedures and Fig. 1B). When reconstituted in the same conditions, apoA-I: 134–145 retained ability to form four out of five particle sizes; with a particle equivalent to the 12.2 nm wild-type being the largest achievable rHDL (Fig. 1B). Interestingly, the largest truncation (apoA-I: 124–155), yielding the shortest apoA-I variant tested, was able to generate a particle equivalent to 12.2 nm wild-type rHDL, but none of the 2-apoA-I-containing rHDL particles (Fig. 1B).

Formation of cholesteryl esters by LCAT in the presence of rHDL particles of different size and protein composition was measured. Consistent with our hypothesis that the region encompassing residues 134–145 predominantly facilitates LCAT activation, the LCAT activation ability of rHDL particles reconstituted with apoA-I: 134–145 was dramatically reduced (Fig. 7), although the apparent size of the particles was not significantly altered (Fig. 1B). In contrast, when residues essential for rHDL formation (124–133 and 146–155) and the structure essential for LCAT activation (134–145) were deleted, both functional (LCAT activation, Fig. 7) and structural (HDL forming ability, Fig. 1B) aspects of HDL were compromised. Notably, by changing the stoichiometry of apoA-I per particle to greater than two apoA-I molecules, the ability of apoA-I: 124–155 to form rHDL was rescued (Fig. 1B, 12.2 nm rHDL), but its LCAT activation function was not (Fig. 7).

DISCUSSION

Despite the prominent antiatherogenic role of apoA-I, the detailed structures of the lipid-free and HDL-associated forms of this protein are largely unknown. Because structural determinants that reside in the central domain of apoA-I are hypothesized to mediate HDL function, a detailed comparative analysis at the single-residue level of the structural adaptation of the central domain of apoA-I upon transition from lipid-free to different subclasses of rHDL may provide insight into how HDL function is modulated in an HDL particle size-dependent fashion. For example, the binding and activation of LCAT is a critical element in cholesterol metabolism and involves residues in helix 4, 5, and 6 (residues 99–164) of HDL-associated apoA-I (63, 66–80). Specific structural features in this domain may influence apoA-I's susceptibility to oxidative reactions that reduce HDL's ability to mediate LCAT activation. These structural details have recently been the subject of much debate (22, 24, 30, 35).

Previously, we examined the conformation of residues within the central domain of apoA-I (61–221) on 9.6 nm rHDL by SDSL-EPR (22). Residues 133 and 146 displayed a high degree of spin coupling suggesting that the single spin-label at these positions is proximal to the analogous spin-label of the paired apoA-I molecule on 9.6 nm rHDL. Furthermore, position 139 showed low spin coupling and an unusually high degree of mobility, suggesting that this residue may be part of a very flexible segment. A model compatible with these observations (the 'looped-belt' model) assigned positions 133 and 146 at the 'hinges' of a loop segment, with 139 at the apex of the loop. According to the 'looped-belt' model,

residues 134–145 are likely poorly lipid-associated and therefore differ from the rest of the residues examined, which form a lipid-associated amphipathic -helical 'belt' circumscribing the rHDL particle perimeter. These hypotheses were supported by fluorescence resonance energy transfer experiments (22), which confirmed that apoA-I on 9.6 nm rHDL forms an anti-parallel association aligned at residue 133.

Subsequent hydrogen-deuterium exchange studies performed by Wu et al. (24) resulted in the 'solar flares' model, in which residues 159–180 compose a large loop region that extends off the surface of 9.6 nm rHDL. In addition to a unique proton exchange profile this loop structure, which resides within the LCAT activation domain, should also have dynamic and polarity properties distinctive from the remainder of apoA-I (rHDL-associated).

To gather more detailed structural information on the loop regions postulated by the 'solar flares' and the 'looped-belt' models , we undertook direct measurements of solvent-accessibility, local polarity, and backbone dynamics for three protein segments (residues 119–124, 139–144, and 164–170) by using site-directed fluorescence and EPR spectroscopies. While both EPR (of site-directed spin labels) and fluorescence (of Trp-substituted residues) measurements have been extensively used to explore lipid-protein interactions independently, a direct comparison of their results for a successively scanned region of protein sequence has not been performed. Therefore we evaluated the complementarity of these methods in determining local charge, backbone structure, and orientation of protein segments associated with lipid particles. These methodologies yielded distinct and complementary information on the local chemistry and dynamics of the targeted positions in apoA-I.

This multi-variable approach provides a robust means of cross-validation and data interpretation. If a residue exhibits biophysical properties that are inconsistent with the prediction of a secondary or tertiary structural model, the apparent outlier value can be reconciled by quantifying other biophysical parameters at the same location.

Taken together, the results reported here support the conclusion that residues 119–124 form a stable lipid-associated amphipathic -helix that is not significantly affected by changes in rHDL particle size. This latter observation is in contrast with the results of the hydrogen-exchange mass-spectrometry study of Chetty et al., which suggest that residues 115–158 do not form a lipid-associated -helix but a disordered loop in 7.8 nm rHDL (34). However, sample preparation was slightly different in the two studies. Whereas in our rHDL preparations we used a small amount of unesterified cholesterol (~4 cholesterol molecules per 7.8 nm rHDL particle), Chetty et al. analyzed cholesterol-free rHDL. The presence of a small amount of cholesterol in rHDL (<6 molecules per particle) facilitates deeper penetration of apolipoproteins into the lipid bilayer with a small increase in helical content (81, 82). Furthermore, residues in the "central domain" of apoA-I are particularly sensitive to the presence of cholesterol (83). While speculative, we propose that the presence of a low molar ratio of cholesterol in our rHDL preparations may be sufficient to stabilize the amphipathic -helical structure of residues 119–124, explaining the discrepancy between our results and those of Chetty et al. (34). Further investigation is necessary to validate this hypothesis.

In the 'looped-belt' model (22) residues 134–145 form a loop dissociated from the lipid bilayer. The current data recapitulate the high degree of spin-coupling for residues 133 and 146 and high mobility for residue 139 on 9.6 nm and 7.8 nm rHDL (Fig. 6), suggesting that the relative alignment of apoA-I on rHDL is not affected by particle size and that the conformation of residues 134–145 is a consistent feature of rHDL-associated apoA-I.

Interestingly, residues 134–145 are comprised in a loop region in the lipid-free form of the protein (84).

For residues 139–144 within the postulated loop, the periodicity of three out of four biophysical parameters suggest that these amino acids do not form an ideal amphipathic α-helical structure in any of the three rHDL subclasses analyzed. Specifically, the side-chain mobility and KI quenching of Trp fluorescence of three positions and the EPR polarity index of two residues out of six did not have the periodicity (3.6 per turn) expected for an ideal amphipathic α-helical structure. These results suggest that either residues 139–144 are non-α-helical or reside on a flexible α-helical segment in rapid association/dissociation dynamics with the edge of the phospholipid bilayer. Importantly, the biophysical properties of residues 139–144 are not rHDL subclass dependent.

A series of computational studies support the hypothesis that apoA-I helix 5 (residues 122–142) in discoidal HDL is loosely associated with the lipid bilayer to form an amphipathic presentation tunnel that assists the transfer of phospholipids and unesterified cholesterol to the active site of LCAT (32, 33). Our current results provide experimental evidence in favor of this hypothesis. The presence of a non-lipid-associated structural motif on rHDL particles of different sizes (7.8, 8.4 and 9.6 nm rHDL), and the ability of these particles to activate LCAT (45) led to the hypothesis that this conserved structural feature facilitates LCAT activation. Results from apoA-I truncation variants suggest that the computationally postulated amphipathic presentation tunnel is the structure (residue 134–145) that we identified experimentally. Notably, deletion of residues 134–145 completely abolished apoA-I's ability to activate LCAT (Fig. 7), without compromising rHDL particle size (Fig. 1), supporting the hypothesis that positions 134–145 reside on a non-lipid associated segment that does not contribute to particle size.

To compare the results obtained for residues 139–144 to another postulated loop region, we extended our analysis to residues 164–170, which in the 'solar-flares' model for 9.6 nm rHDL form an extended loop structure (24). Our biophysical analysis indicates that this region bears unique structural and chemical features. In the lipid-free form of the protein, side-chain mobilities of residues 167 and 170 were the lowest and their polarity indexes the highest of the 19 residues investigated here, suggesting that this region forms a hydrophobic pocket wherein protein-protein contacts significantly restrict side-chain mobility. In contrast however, residue 168 had an unusually high K_{sv} (12.48 M^{-1}; extremely solvent accessible), which is almost two times greater than the next highest value within the residues examined (residue 120, K_{sv}=6.51 M^{-1}). While typically this result would lead to the conclusion that residue 168 is highly exposed to solvent, the three other biophysical parameters examined (side-chain mobility, polarity index, and Trp λ_{max}) do not substantiate this interpretation. Thus, we conclude that the high K_{sv} value for this residue reflects a unique local chemistry rather than an unexpected protein structure.

Although region 164–170 may experience unique tertiary/quaternary structural interactions in the lipid-free form of the protein, our data is consistent with these residues assuming a standard lipid-associated amphipathic α-helical structure when the protein is HDL-associated. This is substantiated by the periodicity of side-chain mobility, polarity index, and Trp λ_{max} for all rHDL subclasses analyzed and by the periodicity of K_{sv} for 7.8 nm rHDL. In contrast, KI quenching results for residues 164 and 165 in 9.6 nm rHDL are inconsistent with an amphipathic α-helical structure. However, KI as a fluorescence quenching probe is highly influenced by local charge, and the microenvironment surrounding positions 164 and 165 is rich in charged residues (R160, R171, D157, D168, and E169). Thus we propose that the K_{sv} values for residues 164 and 165 may be a reflection of the unusual local pK_a in the region.

In conclusion, examination of three unique segments of apoA-I's central domain (residues 119–124, 139–144, 164–170) using four distinct biophysical techniques (Trp $_{max}$, Trp fluorescence KI quenching, polarity index, and side-chain mobility) revealed that while these residues undergo a large structural rearrangement upon lipid association, their lipid-bound conformation is maintained in rHDL particles of different size (7.8 to 9.6 nm). Thus, while discoidal HDL particles may alter their general morphology to accommodate changes in lipids composition (27, 33, 45, 85–87), from our measurements of either backbone/side-chain dynamics or differential accessibility we can conclude that the three regions analyzed retain their secondary structure within the rHDL subclasses examined.

The conservation of the central domain structure on rHDL particles of different size is consistent with the ability of all native HDL particles to activate the LCAT cholesterol esterification reaction. LCAT-mediated lipid polarity changes drive global structural rearrangements and formation of spherical HDL, which likely requires alteration of apoA-I structure and of protein-lipid interactions. Thus it is plausible that the structure of residues 134–145 is conserved in discoidal HDL particles and essential for LCAT activation, but is lost upon formation of spherical HDL, which are poor LCAT activators (88–90). The structure of the central domain in spherical HDL is currently under investigation using a similar multi-technique approach.

Supplementary Material

Refer to Web version on PubMed Central for supplementary material.

Acknowledgments

Abbreviations

The abbreviations used and not defined in text are:

HDL	high density lipoproteins
SDS-PAGE	sodium dodecyl sulfate polyacrylamide gel electrophoresis

REFERENCES

1. Vaisar T, Pennathur S, Green PS, Gharib SA, Hoofnagle AN, Cheung MC, Byun J, Vuletic S, Kassim S, Singh P, Chea H, Knopp RH, Brunzell J, Geary R, Chait A, Zhao XQ, Elkon K, Marcovina S, Ridker P, Oram JF, Heinecke JW. Shotgun proteomics implicates protease inhibition and complement activation in the antiinflammatory properties of HDL. J Clin Invest. 2007; 117:746–756. [PubMed: 17332893]

2. Davidson WS, Silva RA, Chantepie S, Lagor WR, Chapman MJ, Kontush A. Proteomic analysis of defined HDL subpopulations reveals particle-specific protein clusters: relevance to antioxidative function. Arterioscler Thromb Vasc Biol. 2009; 29:870–876. [PubMed: 19325143]

3. Gordon T, Castelli WP, Hjortland MC, Kannel WB, Dawber TR. High density lipoprotein as a protective factor against coronary heart disease. The Framingham Study. Am J Med. 1977; 62:707–714. [PubMed: 193398]

4. Cuchel M, Rader DJ. Macrophage reverse cholesterol transport: key to the regression of atherosclerosis? Circulation. 2006; 113:2548–2555. [PubMed: 16735689]

5. Rothblat GH, Phillips MC. High-density lipoprotein heterogeneity and function in reverse cholesterol transport. Curr Opin Lipidol. 2010; 21:229–238. [PubMed: 20480549]

6. Tabet F, Rye KA. High-density lipoproteins, inflammation and oxidative stress. Clin Sci (Lond). 2009; 116:87–98. [PubMed: 19076062]

7. Sviridov D, Mukhamedova N, Remaley AT, Chin-Dusting J, Nestel P. Antiatherogenic functionality of high density lipoprotein: how much versus how good. J Atheroscler Thromb. 2008; 15:52–62. [PubMed: 18385533]

8. Tall AR. Cholesterol efflux pathways and other potential mechanisms involved in the athero-protective effect of high density lipoproteins. J Intern Med. 2008; 263:256–273. [PubMed: 18271871]

9. Huang R, Silva RA, Jerome WG, Kontush A, Chapman MJ, Curtiss LK, Hodges TJ, Davidson WS. Apolipoprotein A–I structural organization in high-density lipoproteins isolated from human plasma. Nat Struct Mol Biol. 2011; 18:416–422. [PubMed: 21399642]

10. Borhani DW, Rogers DP, Engler JA, Brouillette CG. Crystal structure of truncated human apolipoprotein A–I suggests a lipid-bound conformation. Proc Natl Acad Sci U S A. 1997; 94:12291–12296. [PubMed: 9356442]

11. Segrest JP, Jones MK, Klon AE, Sheldahl CJ, Hellinger M, De Loof H, Harvey SC. A detailed molecular belt model for apolipoprotein A–I in discoidal high density lipoprotein. J Biol Chem. 1999; 274:31755–31758. [PubMed: 10542194]

12. Koppaka V, Silvestro L, Engler JA, Brouillette CG, Axelsen PH. The structure of human lipoprotein A–I. Evidence for the "belt" model. J Biol Chem. 1999; 274:14541–14544. [PubMed: 10329643]

13. Maiorano JN, Davidson WS. The orientation of helix 4 in apolipoprotein A-I-containing reconstituted high density lipoproteins. J Biol Chem. 2000; 275:17374–17380. [PubMed: 10751383]

14. Tricerri MA, Behling Agree AK, Sanchez SA, Jonas A. Characterization of apolipoprotein A–I structure using a cysteine-specific fluorescence probe. Biochemistry. 2000; 39:14682–14691. [PubMed: 11087425]

15. Li H, Lyles DS, Thomas MJ, Pan W, Sorci-Thomas MG. Structural determination of lipid-bound ApoA-I using fluorescence resonance energy transfer. J Biol Chem. 2000; 275:37048–37054. [PubMed: 10956648]

16. Panagotopulos SE, Horace EM, Maiorano JN, Davidson WS. Apolipoprotein A–I adopts a belt-like orientation in reconstituted high density lipoproteins. J Biol Chem. 2001; 276:42965–42970. [PubMed: 11557764]

17. Li HH, Lyles DS, Pan W, Alexander E, Thomas MJ, Sorci-Thomas MG. ApoA-I structure on discs and spheres. Variable helix registry and conformational states. J Biol Chem. 2002; 277:39093–39101. [PubMed: 12167653]

18. Davidson WS, Hilliard GM. The spatial organization of apolipoprotein A–I on the edge of discoidal high density lipoprotein particles: a mass specrometry study. J Biol Chem. 2003; 278:27199–27207. [PubMed: 12724319]

19. Maiorano JN, Jandacek RJ, Horace EM, Davidson WS. Identification and structural ramifications of a hinge domain in apolipoprotein A–I discoidal high-density lipoproteins of different size. Biochemistry. 2004; 43:11717–11726. [PubMed: 15362856]

20. Silva RA, Hilliard GM, Li L, Segrest JP, Davidson WS. A mass spectrometric determination of the conformation of dimeric apolipoprotein A–I in discoidal high density lipoproteins. Biochemistry. 2005; 44:8600–8607. [PubMed: 15952766]

21. Bhat S, Sorci-Thomas MG, Alexander ET, Samuel MP, Thomas MJ. Intermolecular contact between globular N-terminal fold and C-terminal domain of ApoA-I stabilizes its lipid-bound conformation: studies employing chemical cross-linking and mass spectrometry. J Biol Chem. 2005; 280:33015–33025. [PubMed: 15972827]

22. Martin DD, Budamagunta MS, Ryan RO, Voss JC, Oda MN. Apolipoprotein A–I assumes a "looped belt" conformation on reconstituted high density lipoprotein. J Biol Chem. 2006; 281:20418–20426. [PubMed: 16698792]

23. Bhat S, Sorci-Thomas MG, Tuladhar R, Samuel MP, Thomas MJ. Conformational adaptation of apolipoprotein A–I to discretely sized phospholipid complexes. Biochemistry. 2007; 46:7811–7821. [PubMed: 17563120]

24. Wu Z, Wagner MA, Zheng L, Parks JS, Shy JM, Smith JD 3rd, Gogonea V, Hazen SL. The refined structure of nascent HDL reveals a key functional domain for particle maturation and dysfunction. Nat Struct Mol Biol. 2007; 14:861–868. [PubMed: 17676061]

25. Silva RA, Huang R, Morris J, Fang J, Gracheva EO, Ren G, Kontush A, Jerome WG, Rye KA, Davidson WS. Structure of apolipoprotein A–I in spherical high density lipoproteins of different sizes. Proc Natl Acad Sci U S A. 2008; 105:12176–12181. [PubMed: 18719128]

26. Gu F, Jones MK, Chen J, Patterson JC, Catte A, Jerome WG, Li L, Segrest JP. Structures of discoidal high density lipoproteins: a combined computational-experimental approach. J Biol Chem. 2010; 285:4652–4665. [PubMed: 19948731]

27. Sorci-Thomas MG, Owen JS, Fulp B, Bhat S, Zhu X, Parks JS, Shah D, Jerome WG, Gerelus M, Zabalawi M, Thomas MJ. Nascent high density lipoproteins formed by ABCA1 resemble lipid rafts and are structurally organized by three apoA-I monomers. J Lipid Res. 2012; 53:1890–1909. [PubMed: 22750655]

28. Wu Z, Gogonea V, Lee X, Wagner MA, Li XM, Huang Y, Undurti A, May RP, Haertlein M, Moulin M, Gutsche I, Zaccai G, Didonato JA, Hazen SL. Double superhelix model of high density lipoprotein. J Biol Chem. 2009; 284:36605–36619. [PubMed: 19812036]

29. Gogonea V, Wu Z, Lee X, Pipich V, Li XM, Ioffe AI, Didonato JA, Hazen SL. Congruency between biophysical data from multiple platforms and molecular dynamics simulation of the double-super helix model of nascent high-density lipoprotein. Biochemistry. 2010; 49:7323–7343. [PubMed: 20687589]

30. Jones MK, Zhang L, Catte A, Li L, Oda MN, Ren G, Segrest JP. Assessment of the validity of the double superhelix model for reconstituted high density lipoproteins: a combined computational-experimental approach. J Biol Chem. 2010; 285:41161–41171. [PubMed: 20974855]

31. Corsico B, Toledo JD, Garda HA. Evidence for a central apolipoprotein A–I domain loosely bound to lipids in discoidal lipoproteins that is capable of penetrating the bilayer of phospholipid vesicles. J Biol Chem. 2001; 276:16978–16985. [PubMed: 11278925]

32. Klon AE, Segrest JP, Harvey SC. Molecular dynamics simulations on discoidal HDL particles suggest a mechanism for rotation in the apo A–I belt model. J Mol Biol. 2002; 324:703–721. [PubMed: 12460572]

33. Jones MK, Catte A, Li L, Segrest JP. Dynamics of activation of lecithin:cholesterol acyltransferase by apolipoprotein A–I. Biochemistry. 2009; 48:11196–11210. [PubMed: 19860440]

34. Sevugan Chetty P, Mayne L, Kan ZY, Lund-Katz S, Englander SW, Phillips MC. Apolipoprotein A–I helical structure and stability in discoidal high-density lipoprotein (HDL) particles by hydrogen exchange and mass spectrometry. Proc Natl Acad Sci U S A. 2012; 109:11687–11692. [PubMed: 22745166]

35. Shih AY, Sligar SG, Schulten K. Molecular models need to be tested: the case of a solar flares discoidal HDL model. Biophys J. 2008; 94:L87–L89. [PubMed: 18375520]

36. Duong PT, Weibel GL, Lund-Katz S, Rothblat GH, Phillips MC. Characterization and properties of pre beta-HDL particles formed by ABCA1-mediated cellular lipid efflux to apoA-I. J Lipid Res. 2008; 49:1006–1014. [PubMed: 18252847]

37. Wroblewska M. The origin and metabolism of a nascent pre-beta high density lipoprotein involved in cellular cholesterol efflux. Acta Biochim Pol. 2011; 58:275–285. [PubMed: 21750785]

38. Kammann M, Laufs J, Schell J, Gronenborn B. Rapid insertional mutagenesis of DNA by polymerase chain reaction (PCR). Nucleic Acids Res. 1989; 17:5404. [PubMed: 2548160]

39. Cavigiolio G, Geier EG, Shao B, Heinecke JW, Oda MN. Exchange of apolipoprotein A–I between lipid-associated and lipid-free states: a potential target for oxidative generation of dysfunctional high density lipoproteins. J Biol Chem. 2010; 285:18847–18857. [PubMed: 20385548]

40. Ryan RO, Forte TM, Oda MN. Optimized bacterial expression of human apolipoprotein A–I. Protein Expr Purif. 2003; 27:98–103. [PubMed: 12509990]

41. Oda MN, Forte TM, Ryan RO, Voss JC. The C-terminal domain of apolipoprotein A–I contains a lipid-sensitive conformational trigger. Nat Struct Biol. 2003; 10:455–460. [PubMed: 12754494]

42. Lagerstedt JO, Cavigiolio G, Budamagunta MS, Pagani I, Voss JC, Oda MN. Structure of apolipoprotein A–I N terminus on nascent high density lipoproteins. J Biol Chem. 2011; 286:2966–2975. [PubMed: 21047795]

43. Nichols AV, Gong EL, Blanche PJ, Forte TM. Characterization of discoidal complexes of phosphatidylcholine, apolipoprotein A–I and cholesterol by gradient gel electrophoresis. Biochim Biophys Acta. 1983; 750:353–364. [PubMed: 6407531]

44. Nichols AV, Gong EL, Blanche PJ, Forte TM, Shore VG. Pathways in the formation of human plasma high density lipoprotein subpopulations containing apolipoprotein A–I without apolipoprotein A–II. J Lipid Res. 1987; 28:719–732. [PubMed: 3112299]

45. Cavigiolio G, Shao B, Geier EG, Ren G, Heinecke JW, Oda MN. The interplay between size, morphology, stability, and functionality of high-density lipoprotein subclasses. Biochemistry. 2008; 47:4770–4779. [PubMed: 18366184]

46. Burstein EA, Vedenkina NS, Ivkova MN. Fluorescence and the location of tryptophan residues in protein molecules. Photochem Photobiol. 1973; 18:263–279. [PubMed: 4583619]

47. Davidson WS, Arnvig-McGuire K, Kennedy A, Kosman J, Hazlett TL, Jonas A. Structural organization of the N-terminal domain of apolipoprotein A–I: studies of tryptophan mutants. Biochemistry. 1999; 38:14387–14395. [PubMed: 10572013]

48. Beckstead JA, Block BL, Bielicki JK, Kay CM, Oda MN, Ryan RO. Combined N- and C-terminal truncation of human apolipoprotein A–I yields a folded, functional central domain. Biochemistry. 2005; 44:4591–4599. [PubMed: 15766290]

49. Phu MJ, Hawbecker SK, Narayanaswami V. Fluorescence resonance energy transfer analysis of apolipoprotein E C-terminal domain and amyloid beta peptide (1–42) interaction. J Neurosci Res. 2005; 80:877–886. [PubMed: 15880461]

50. Saito H, Dhanasekaran P, Nguyen D, Holvoet P, Lund-Katz S, Phillips MC. Domain structure and lipid interaction in human apolipoproteins A–I and E, a general model. J Biol Chem. 2003; 278:23227–23232. [PubMed: 12709430]

51. Chapman, SK.; Reid, GA. Flavoprotein Protocols. Humana Press; 1999.

52. Lakowicz, JR. Principles of fluorescence spectroscopy. 3rd ed.. New York: Springer; 2006.

53. Lehrer SS. Solute perturbation of protein fluorescence. The quenching of the tryptophyl fluorescence of model compounds and of lysozyme by iodide ion. Biochemistry. 1971; 10:3254–3263. [PubMed: 5119250]

54. Froncisz W, Hyde JS. The loop-gap resonator: A new microwave lumped circuit ESR sample structure. J Magn Reson. 1982; 47:515–521.

55. Hubbell WL, Froncisz W, Hyde JS. Continuous and stopped flow EPR spectrometer based on a loop gap resonator. Rev Sci Instrum. 1987; 58:1879–1886.

56. Oh KJ, Altenbach C, Collier RJ, Hubbell WL. Site-directed spin labeling of proteins. Applications to diphtheria toxin. Methods Mol Biol. 2000; 145:147–169. [PubMed: 10820721]

57. Altenbach C, Greenhalgh DA, Khorana HG, Hubbell WL. A collision gradient method to determine the immersion depth of nitroxides in lipid bilayers: application to spin-labeled mutants of bacteriorhodopsin. Proc Natl Acad Sci U S A. 1994; 91:1667–1671. [PubMed: 8127863]

58. Klug CS, Su W, Feix JB. Mapping of the residues involved in a proposed beta-strand located in the ferric enterobactin receptor FepA using site-directed spin-labeling. Biochemistry. 1997; 36:13027–13033. [PubMed: 9335564]

59. Klug CS, Feix JB. Methods and applications of site-directed spin labeling EPR spectroscopy. Methods Cell Biol. 2008; 84:617–658. [PubMed: 17964945]

60. Ball A, Nielsen R, Gelb MH, Robinson BH. Interfacial membrane docking of cytosolic phospholipase A2 C2 domain using electrostatic potential-modulated spin relaxation magnetic resonance. Proc Natl Acad Sci U S A. 1999; 96:6637–6642. [PubMed: 10359764]

61. Shao B, Cavigiolio G, Brot N, Oda MN, Heinecke JW. Methionine oxidation impairs reverse cholesterol transport by apolipoprotein A–I. Proc Natl Acad Sci U S A. 2008; 105:12224–12229. [PubMed: 18719109]

62. Andrews AL, Atkinson D, Barratt MD, Finer EG, Hauser H, Henry R, Leslie RB, Owens NL, Phillips MC, Robertson RN. Interaction of apoprotein from porcine high-density lipoprotein with

dimyristoly lecithin. 2. Nature of lipid-protein interaction. Eur J Biochem. 1976; 64:549–563. [PubMed: 179816]

63. Segrest JP, Jones MK, De Loof H, Brouillette CG, Venkatachalapathi YV, Anantharamaiah GM. The amphipathic helix in the exchangeable apolipoproteins: a review of secondary structure and function. J Lipid Res. 1992; 33:141–166. [PubMed: 1569369]

64. Jayaraman S, Abe-Dohmae S, Yokoyama S, Cavigiolio G. Impact of self-association on function of apolipoprotein A–I. J Biol Chem. 2011; 286:35610–35623. [PubMed: 21835924]

65. McHaourab HS, Lietzow MA, Hideg K, Hubbell WL. Motion of spin-labeled side chains in T4 lysozyme. Correlation with protein structure and dynamics. Biochemistry. 1996; 35:7692–7704. [PubMed: 8672470]

66. Cho KH, Durbin DM, Jonas A. Role of individual amino acids of apolipoprotein A–I in the activation of lecithin:cholesterol acyltransferase and in HDL rearrangements. J Lipid Res. 2001; 42:379–389. [PubMed: 11254750]

67. Roosbeek S, Vanloo B, Duverger N, Caster H, Breyne J, De Beun I, Patel H, Vandekerckhove J, Shoulders C, Rosseneu M, Peelman F. Three arginine residues in apolipoprotein A–I are critical for activation of lecithin:cholesterol acyltransferase. J Lipid Res. 2001; 42:31–40. [PubMed: 11160363]

68. Chroni A, Kan HY, Kypreos KE, Gorshkova IN, Shkodrani A, Zannis VI. Substitutions of glutamate 110 and 111 in the middle helix 4 of human apolipoprotein A–I (apoA-I) by alanine affect the structure and in vitro functions of apoA-I and induce severe hypertriglyceridemia in apoA-I-deficient mice. Biochemistry. 2004; 43:10442–10457. [PubMed: 15301543]

69. Banka CL, Bonnet DJ, Black AS, Smith RS, Curtiss LK. Localization of an apolipoprotein A–I epitope critical for activation of lecithin-cholesterol acyltransferase. J Biol Chem. 1991; 266:23886–23892. [PubMed: 1721059]

70. Meng QH, Calabresi L, Fruchart JC, Marcel YL. Apolipoprotein A–I domains involved in the activation of lecithin:cholesterol acyltransferase. Importance of the central domain. J Biol Chem. 1993; 268:16966–16973. [PubMed: 7688720]

71. Sorci-Thomas M, Kearns MW, Lee JP. Apolipoprotein A–I domains involved in lecithin-cholesterol acyltransferase activation. Structure:function relationships. J Biol Chem. 1993; 268:21403–21409. [PubMed: 8407982]

72. Holvoet P, Zhao Z, Vanloo B, Vos R, Deridder E, Dhoest A, Taveirne J, Brouwers E, Demarsin E, Engelborghs Y, et al. Phospholipid binding and lecithin-cholesterol acyltransferase activation properties of apolipoprotein A–I mutants. Biochemistry. 1995; 34:13334–13342. [PubMed: 7577918]

73. Uboldi P, Spoladore M, Fantappie S, Marcovina S, Catapano AL. Localization of apolipoprotein A–I epitopes involved in the activation of lecithin:cholesterol acyltransferase. J Lipid Res. 1996; 37:2557–2568. [PubMed: 9017508]

74. Dhoest A, Zhao Z, De Geest B, Deridder E, Sillen A, Engelborghs Y, Collen D, Holvoet P. Role of the Arg123-Tyr166 paired helix of apolipoprotein A–I in lecithin:cholesterol acyltransferase activation. J Biol Chem. 1997; 272:15967–15972. [PubMed: 9188498]

75. Sorci-Thomas MG, Curtiss L, Parks JS, Thomas MJ, Kearns MW. Alteration in apolipoprotein A–I 22-mer repeat order results in a decrease in lecithin:cholesterol acyltransferase reactivity. J Biol Chem. 1997; 272:7278–7284. [PubMed: 9054424]

76. Sorci-Thomas MG, Curtiss L, Parks JS, Thomas MJ, Kearns MW, Landrum M. The hydrophobic face orientation of apolipoprotein A–I amphipathic helix domain 143–164 regulates lecithin:cholesterol acyltransferase activation. J Biol Chem. 1998; 273:11776–11782. [PubMed: 9565601]

77. McManus DC, Scott BR, Frank PG, Franklin V, Schultz JR, Marcel YL. Distinct central amphipathic alpha-helices in apolipoprotein A–I contribute to the in vivo maturation of high density lipoprotein by either activating lecithin-cholesterol acyltransferase or binding lipids. J Biol Chem. 2000; 275:5043–5051. [PubMed: 10671546]

78. Alexander ET, Bhat S, Thomas MJ, Weinberg RB, Cook VR, Bharadwaj MS, Sorci-Thomas M. Apolipoprotein A–I helix 6 negatively charged residues attenuate lecithin-cholesterol acyltransferase (LCAT) reactivity. Biochemistry. 2005; 44:5409–5419. [PubMed: 15807534]

79. Frank PG, N'Guyen D, Franklin V, Neville T, Desforges M, Rassart E, Sparks DL, Marcel YL. Importance of central alpha-helices of human apolipoprotein A–I in the maturation of high-density lipoproteins. Biochemistry. 1998; 37:13902–13909. [PubMed: 9753480]

80. Yokoyama S, Fukushima D, Kupferberg JP, Kezdy FJ, Kaiser ET. The mechanism of activation of lecithin:cholesterol acyltransferase by apolipoprotein A–I and an amphiphilic peptide. J Biol Chem. 1980; 255:7333–7339. [PubMed: 6771289]

81. Massey JB, Pownall HJ. Role of oxysterol structure on the microdomain-induced microsolubilization of phospholipid membranes by apolipoprotein A–I. Biochemistry. 2005; 44:14376–14384. [PubMed: 16245954]

82. Sparks DL, Davidson WS, Lund-Katz S, Phillips MC. Effect of cholesterol on the charge and structure of apolipoprotein A–I in recombinant high density lipoprotein particles. J Biol Chem. 1993; 268:23250–23257. [PubMed: 8226847]

83. Bergeron J, Frank PG, Scales D, Meng QH, Castro G, Marcel YL. Apolipoprotein A–I conformation in reconstituted discoidal lipoproteins varying in phospholipid and cholesterol content. J Biol Chem. 1995; 270:27429–27438. [PubMed: 7499199]

84. Lagerstedt JO, Budamagunta MS, Liu GS, DeValle NC, Voss JC, Oda MN. The "beta-clasp" model of apolipoprotein A-I--a lipid-free solution structure determined by electron paramagnetic resonance spectroscopy. Biochim Biophys Acta. 2012; 1821:448–455. [PubMed: 22245143]

85. Catte A, Patterson JC, Jones MK, Jerome WG, Bashtovyy D, Su Z, Gu F, Chen J, Aliste MP, Harvey SC, Li L, Weinstein G, Segrest JP. Novel changes in discoidal high density lipoprotein morphology: a molecular dynamics study. Biophys J. 2006; 90:4345–4360. [PubMed: 16581834]

86. Jones MK, Catte A, Patterson JC, Gu F, Chen J, Li L, Segrest JP. Thermal stability of apolipoprotein A–I in high-density lipoproteins by molecular dynamics. Biophys J. 2009; 96:354–371. [PubMed: 19167289]

87. Miyazaki M, Nakano M, Fukuda M, Handa T. Smaller discoidal high-density lipoprotein particles form saddle surfaces, but not planar bilayers. Biochemistry. 2009; 48:7756–7763. [PubMed: 19610670]

88. Jonas A, Wald JH, Toohill KL, Krul ES, Kezdy KE. Apolipoprotein A–I structure and lipid properties in homogeneous, reconstituted spherical and discoidal high density lipoproteins. J Biol Chem. 1990; 265:22123–22129. [PubMed: 2125044]

89. Jonas A. Lecithin-cholesterol acyltransferase in the metabolism of high-density lipoproteins. Biochim Biophys Acta. 1991; 1084:205–220. [PubMed: 1888769]

90. Rye KA, Clay MA, Barter PJ. Remodelling of high density lipoproteins by plasma factors. Atherosclerosis. 1999; 145:227–238. [PubMed: 10488948]
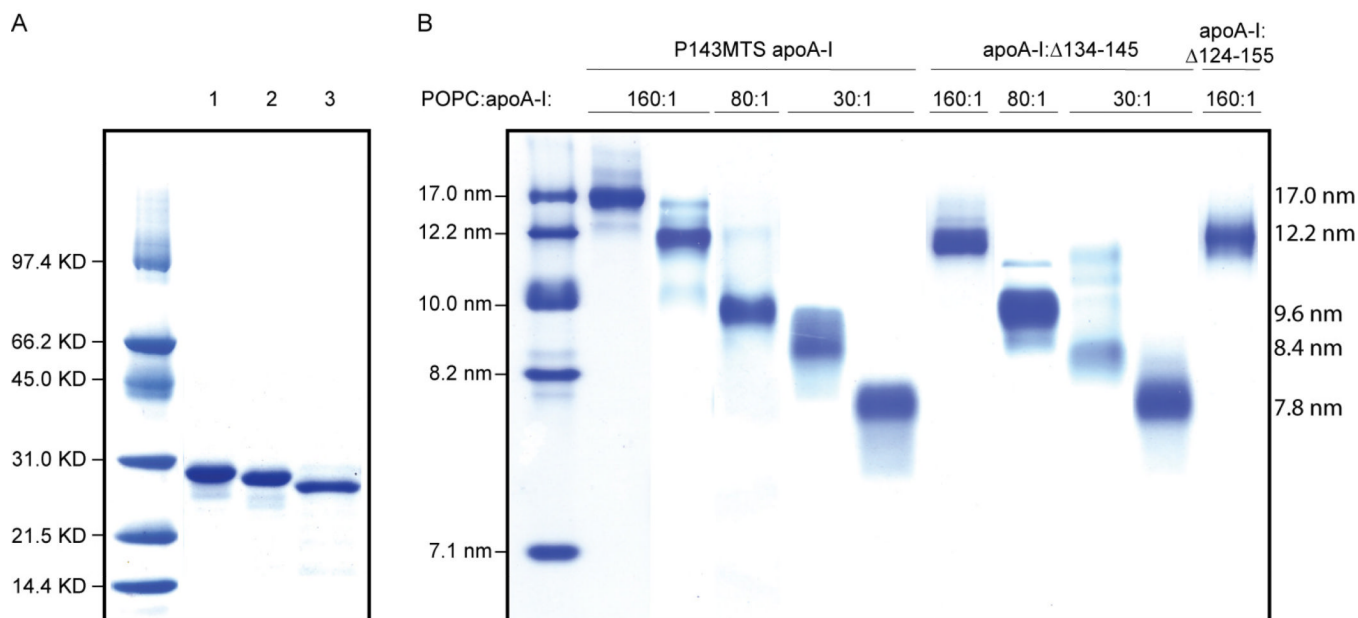
Fig. 1.
Panel A, PAGE-SDS analysis of a full-length apoA-I variant (lane 1, spin-labeled P143C apoA-I is representative of the 40 full-length protein variants analyzed) and truncation variants apoA-I: 134–145 (lane 2) and apoA-I: 124–155 (lane 3). Panel B, NDGGE analysis of purified rHDL subclasses obtained by spin-labeled P143C apoA-I (representative of the 40 full length apoA-I variants) and truncation variants apoA-I: 134–145 and apoA-I: 124–155. Wild-type apoA-I (see reference (45)) and all full-length apoA-I variants were capable of forming five rHDL subclasses. Four rHDL subclasses were generated by apoA-I: 134–145; no rHDL larger than 12.2 nm was reconstituted. Lipidation of apoA-I: 124–155 resulted only in the production of ~12.2 nm rHDL.
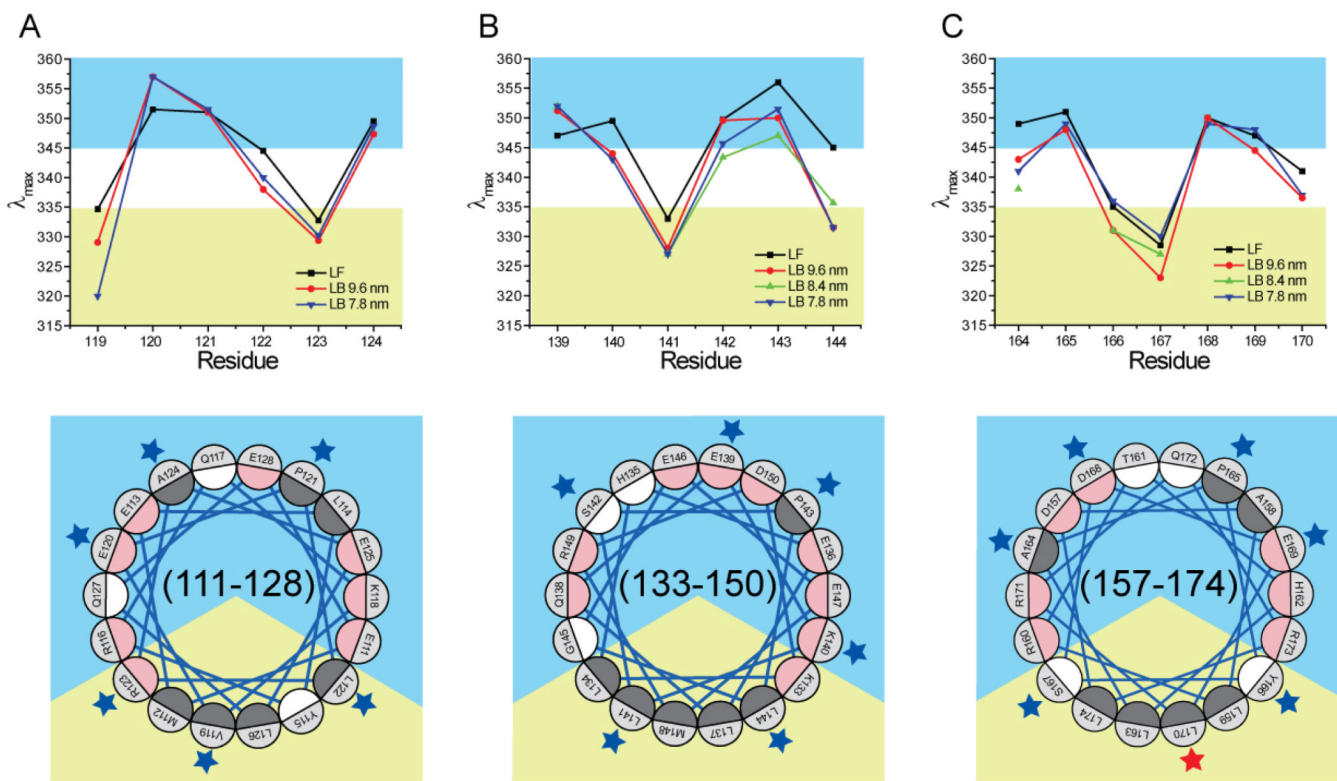
Fig. 2.
Maximum fluorescence emission wavelength (λ_{max}) of residues 119–124 (panel A), 139–144 (panel B), and 164–170 (panel C). Bottom quadrants are 18/5 pitch Schiffer-Edmunson helical wheel diagrams of regions 111–128, 133–150, and 157–174. Residues were color coded according to side chain polarities: dark grey for hydrophobic, white for polar and uncharged, and pink for charged residues. The orientation of the amphipathic wheels was solely based on clustering of hydrophobic residue on a sector of the wheel. The apolar and polar solvation space were color-coded yellow and blue, respectively. Residues 119–124, 139–144, and 164–170 are marked by blue or red stars if their λ_{max} is or is not consistent with a lipid-associated amphipathic α-helix conformation, respectively.
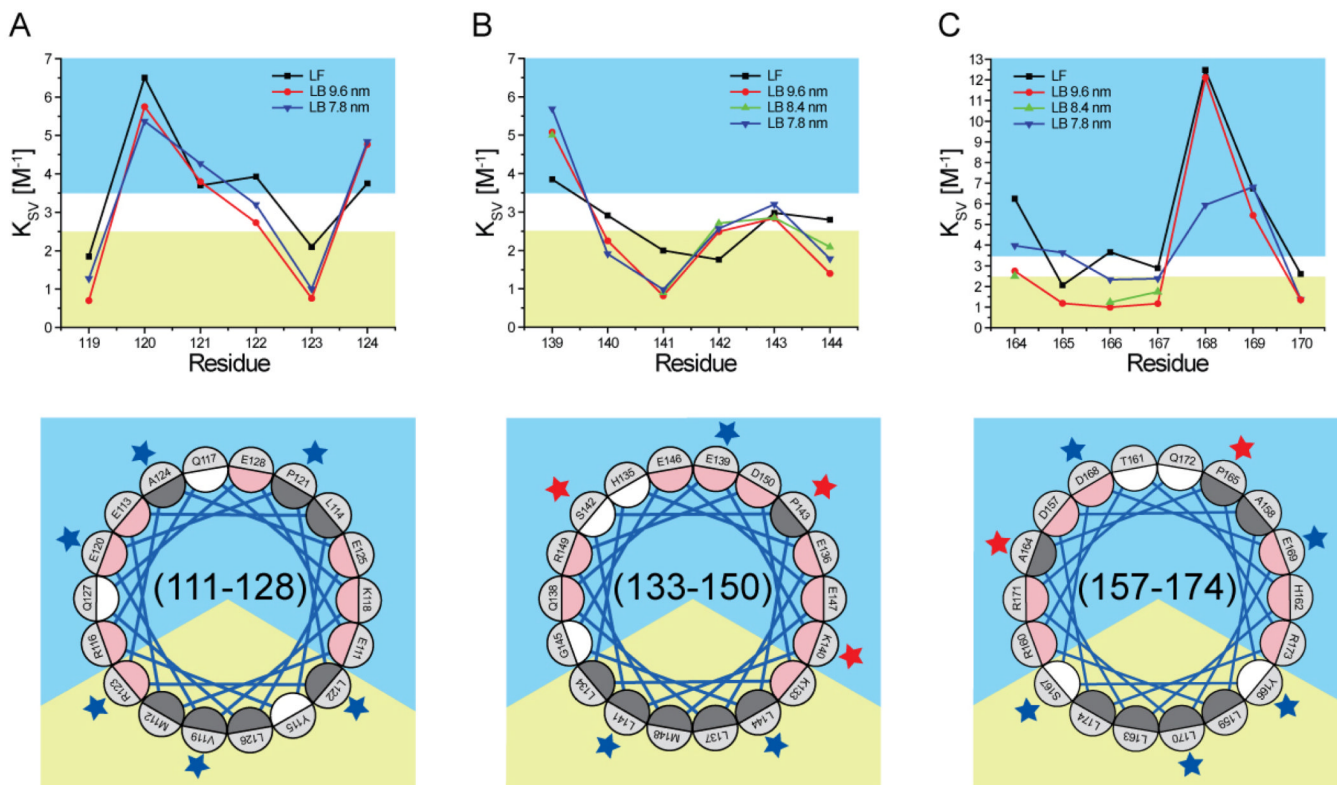
Fig. 3.
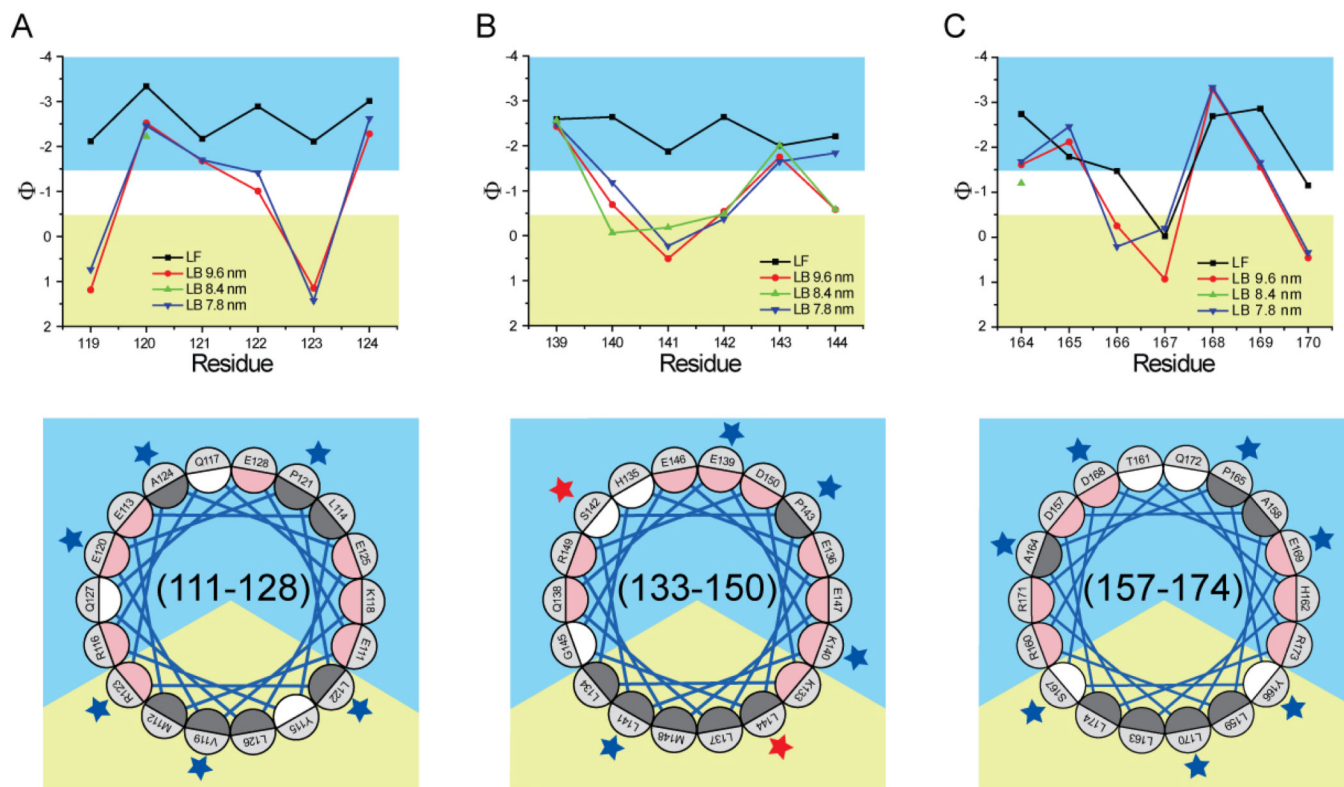Stern-Volmer constant (K_{sv}) of residues 119–124 (panel A), 139–144 (panel B), and 164–170 (panel C). Bottom quadrants are Schiffer-Edmunson helical wheel diagrams of regions 111–128, 133–150, and 157–174 oriented and color-coded as explained in legend to Fig. 2. Residues 119–124, 139–144, and 164–170 are marked by blue or red stars if their K_{sv} is or is not consistent with a lipid-associated amphipathic -helix conformation, respectively.

Fig. 4.
Polarity index ( ) of residues 119–124 (panel A), 139–144 (panel B), and 164–170 (panel C). Bottom quadrants are Schiffer-Edmunson helical wheel diagrams of regions 111–128, 133–150, and 157–174 oriented and color-coded as explained in legend to Fig. 2. Residues 119–124, 139–144, and 164–170 are marked by blue or red stars if their polarity index is or is not consistent with a lipid-associated amphipathic -helix conformation, respectively.
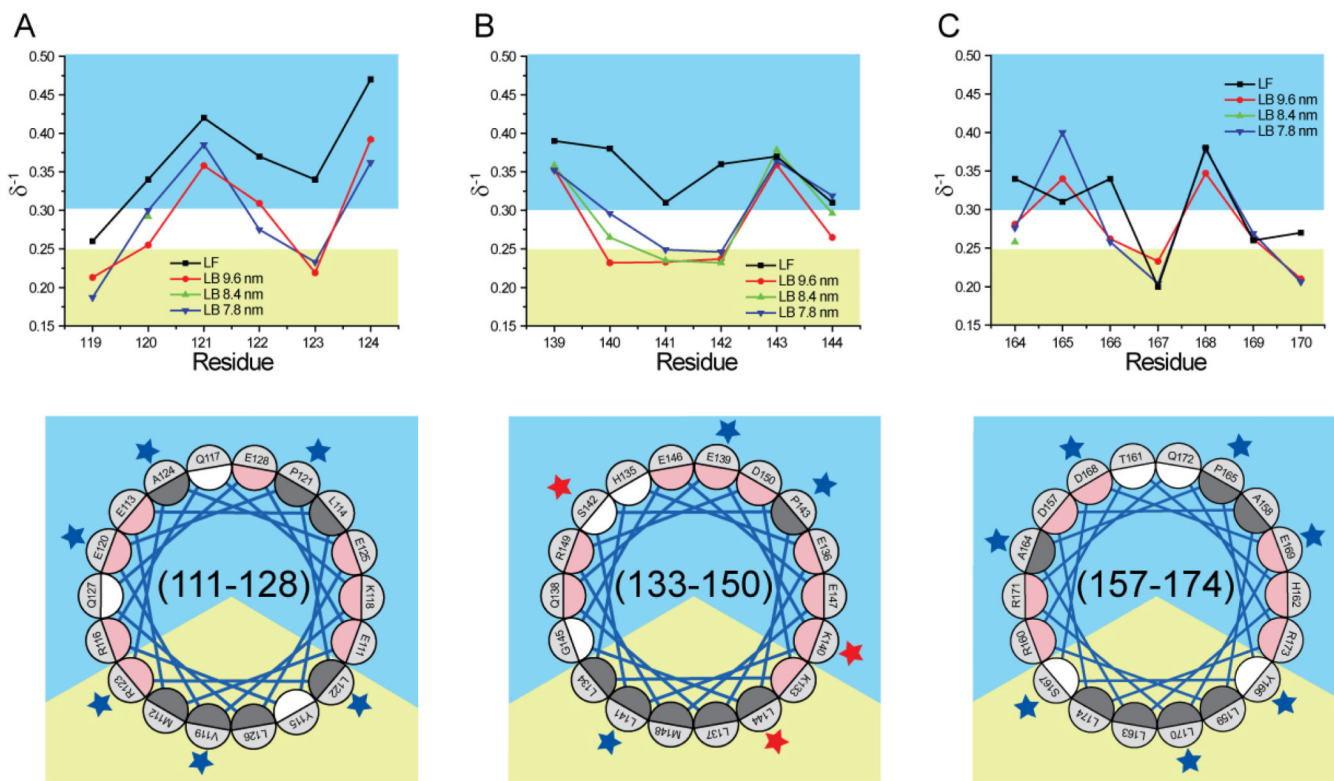
Fig. 5.
Mobility parameter (δ^{-1}) of residues 119–124 (panel A), 139–144 (panel B), and 164–170 (panel C). Bottom quadrants are Schiffer-Edmunson helical wheel diagrams of regions 111–128, 133–150, and 157–174 oriented and color-coded as explained in legend to Fig. 2. Residues 119–124, 139–144, and 164–170 are marked by blue or red stars if their mobility score is or is not consistent with a lipid-associated amphipathic α-helix conformation, respectively.
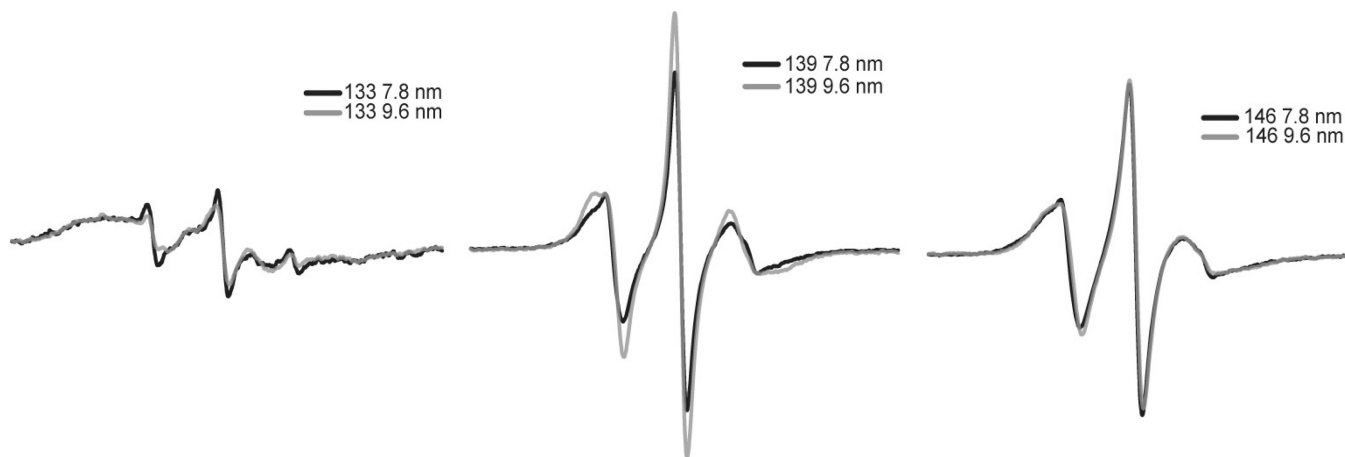
Fig. 6.
EPR spectra of spin-labeled K133C, E139C, and E146C apoA-I variants, in 7.8 nm (black) and 9.6 nm (gray) rHDL.
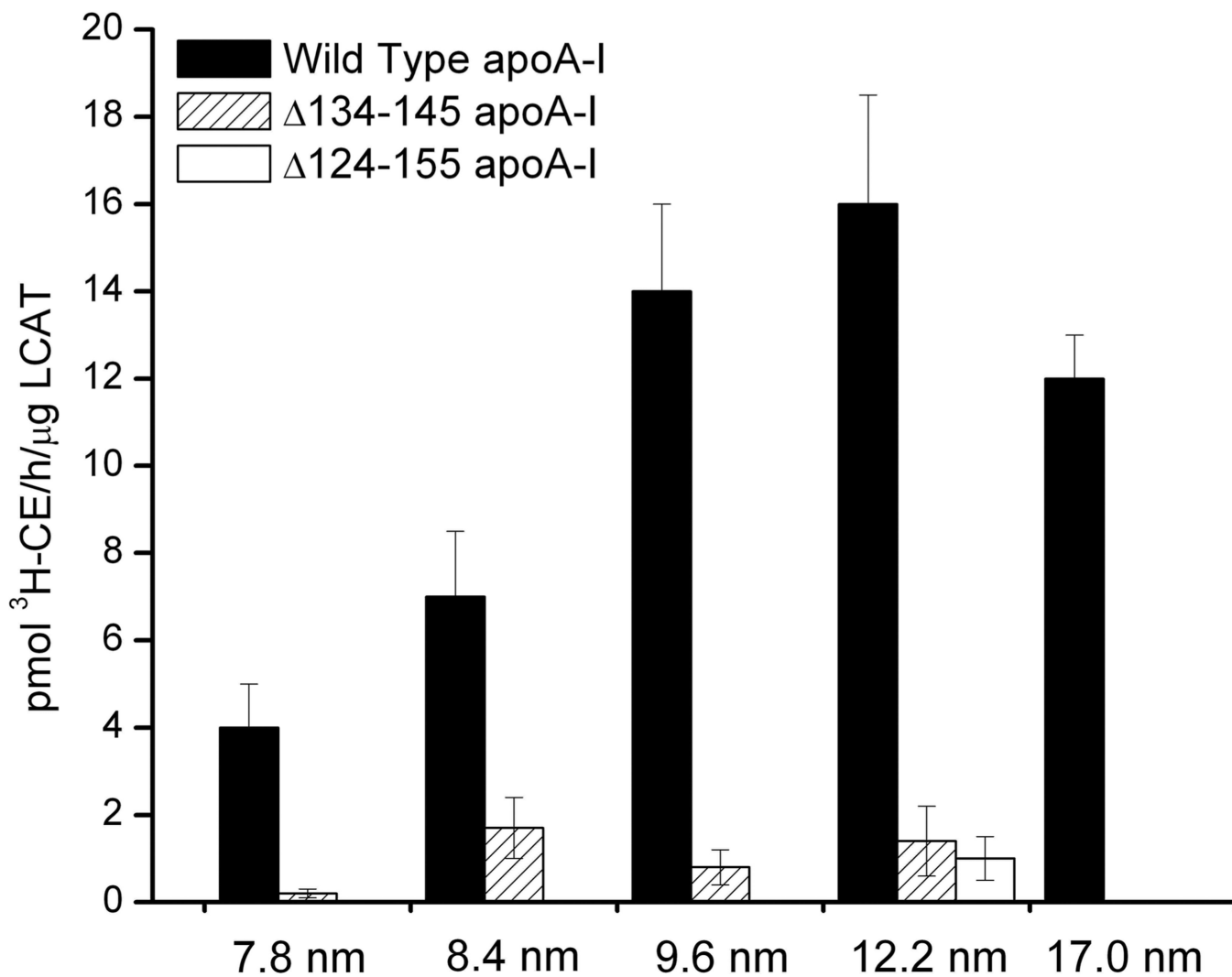
Fig. 7.
LCAT activation by wild-type rHDL (5 particle sizes), 134–145 apoA-I rHDL (4 particle sizes), and 124–155 apoA-I rHDL (12.2 nm rHDL only). Mean and standard deviation (error bars) results are from three independent experiments.